CHAPTER IV
MORPHOLOGICAL AND ELECTROCHEMICAL STUDY OF IRON OXIDE/CARBON XEROGEL NANOCOMPOSITES FOR SUPERCAPACITOR

4.1 Abstract

A hybrid composite electrode for supercapacitor has been prepared from iron oxide and nanoporous carbon derived from polybenzoxazine. First, porous polybenzoxazine was prepared through a sol-gel process before pyrolysis under nitrogen gas at high temperature yielding nanoporous carbon. In order to improve an electrochemical performance of the electrodes, nanoporous carbon was underwent the heat treatment at 300 °C in air to improve the wettability of the electrolyte on the surface of porous carbon. The BET surface area of the heat–treated carbon xerogel was approximately 372 m^2/g. The cyclic voltammeter, galvanostatic charge/discharge, and electrochemical impedance spectroscopy were used to investigate the electrode performance. The results showed that the electrodes prepared from polybenzoxazine-derived-carbon xerogel exhibited good electrochemical performance. A specific capacitance of the heat–treated carbon xerogel electrodes was 108 F/g obtained in 6M KOH at current density 5 mA/cm^2. In addition to the effect of the nanoporous carbon microstructure, the effect of iron oxide (Fe_3O_4) content (1, 3, and 5 wt.%) on the electrochemical properties of the composite electrodes was also investigated. Electrochemical characterization indicated that 3 wt.% Fe_3O_4–impregnated carbon xerogel with heat treatment showed the highest specific capacitance (120 F/g) due to the pseudocapacitive properties of iron oxide. The electrochemical impedance spectroscopy and cyclic voltammetry were also confirmed this electrochemical behavior.

Keywords: Carbon xerogel/ Iron oxide/ Nanoporous carbon/ Polybenzoxazine/ Supercapacitor

4.2 Introduction

The supercapacitor is an electrochemical energy–storage device that is invented to respond to the increasing demand for energy. It can be used as the energy–storage systems for electric vehicles, electronic devices, back-up sources, etc. Great attentions of this device over batteries, capacitors, and fuel cells have been focused on their high specific capacitance, high energy density, long life-cycle, low cost, and environmental friendliness [1].

Generally, the electrochemical supercapasitors can be classified into two types according to the charge/discharge mechanism; electrochemical double–layer capacitors (EDLCs) and pseudocapacitors. EDLCs store energy via electrostatic adsorption/desorption in which charge is divided at the interface of electrode and electrolyte; on the other hand, pseudocapacitors store energy by faradaic redox reactions through metal oxides which are formed on the electrode surface. These materials are also electroactive materials. Among many metal oxides, ruthenium oxide (RuO_2) is a promising material but its rarity and high cost are impractical for commercial scale [2]. In fact, the metal oxides are not only the major material studied for capacitors, but carbon and conducting polymers were also investigated [3]. Carbon aerogels have received great attention as the electrode materials due to their useful properties such as high porosity, high surface area, outstanding electrical conductivity, easily accessible [4].

The polycondensation of resocinal and formaldehyde has been generally used for the carbon aerogels preparation because the physical properties of carbon aerogels can be easily controlled via modification of preparation conditions, for instance, concentrations, pHs, reaction times, and temperatures. However, carbon aerogels are generally obtained by supercritical drying which is inappropriate for commercialization due to high cost. Therefore, ambient drying process has been focused instead to obtain carbon aerogels [5] and the carbon obtained via ambient drying is generally called "carbon xerogel". In this work, polybenzoxazine, a novel type of phenolic resin, was selected as a precursor for the preparation of carbon xerogel owing to its unique characteristics, e.g., excellent dimensional stability, low shrinkage upon polymerization and low water adsorption. Furthermore, the

molecular design flexibility allows the tailoring of the cured materials properties in order to fit desired applications [6].

The purposes of this work are to find out the optimum doping amount of metal oxide on the electrode surface and to evaluate the effect of metal oxide on the electrochemical properties.

4.3 Experimental

4.3.1 Materials

All chemicals were used without further purification. Bisphenol-A was purchased from Aldrich, Germany. Triethylenetetramine (TETA) was purchased from FACAI Group Limited, Thailand. Formaldehyde solution (37% by weight) and potassium hydroxide (KOH analytical grade) were purchased from Merck, Germany. *N,N*-Dimethlyformamide (DMF) was purchased from Labscan Asia Co., Ltd., Thailand. Ferrous chloride hexahydrate ($FeCl_3 \cdot 6H_2O$) and ferrous chloride tetrahydrate ($FeCl_2 \cdot 4H_2O$) were purchased from Fluka, Germany. Ammonium hydroxide (NH_4OH) was purchased Panreac Quimica Sau.

4.3.2 Measurements

Thermal behaviors of polybenzoxazine aerogel were determined with differential scanning calorimetry (DSC), Perkin Elmer DSC7; The sample was heated from ambient temperature to 300 °C at a heating rate of 10 °C/min under nitrogen flow rate of 10 ml/min. Thermogravimetric analysis was also conducted with Perkin Elmer Thermogravimetric/Differential Thermal Analyzer (TG-DTA) where the sample was heated from ambient temperature to 900 °C at a heating rate of 20 °C/min under nitrogen flow rate of 50 ml/min. FT-IR spectra of polybenzoxazine precursor and carbon xerogel were recorded on a Nicolet Nexus 670 FT-IR spectrometer using KBr pallet technique. The field emission scanning electron microscope (FE-SEM, HITACHI S4800) was used to study the microstructure of carbon xerogel, the samples were coated with platinum under vacuum prior to investigation. BET surface area and pore size distribution of all carbon xerogels were calculated from nitrogen adsorption isotherms at 77 K using a Quantachrome/Autosorb-1 Surface Area Analyzer based on the Brunauer–Emmett–

Teller (BET) and Barret-Joyner-Halenda (BJH) methods, respectively. X-Ray Diffractometer (XRD) was used to characterize the crystalline structure of iron oxide (Fe_3O_4). For all electrochemical measurements, the electrochemical test cell consisted of graphite sheets as current collectors and two carbon xerogel or two hybrid composite electrodes separated by microporous polyethylene membrane. The electrodes were soaked in 6M potassium hydroxide (KOH) electrolyte for 24 hr before measurement to ensure complete filling of the porous electrodes [7, 8]. The electrochemical properties were measured by a computer-controlled potentiotat/galvanostat (Autolab PG-STAT 30 with GPES software). Cyclic voltammograms were performed in the potential range of -1.0 V to 1.0 V with various scan rates. For galvanostatic charge/discharge measurement, the testing cell was charged with current density of 5 mA/cm^2 up to 1 V and discharged with 5 mA/cm^2 down to 0 V [7]. Electrochemical impedance spectroscopy measurements were carried out by Autolab PG-STAT 30 with FRA software in the frequency range of 10 kHz to 10 mHz with a sinusoidal signal of 10 mV. All of the electrochemical measurements were performed at room temperature.

4.3.3 Methodology

4.3.3.1 Synthesis of Polybenzoxazine Xerogels

Polybenzoxazine precursor was synthesized by dissolving bisphenol-A (2.30 g) in *N,N*,-dimethylformamide (DMF) (15.00 g) and stirring continuously. Formaldehyde solution (3.28 g) was then added into bisphenol-A solution. The solution was kept under low temperature by using ice bath. TETA (1.74 g) was subsequently added dropwise into the mixture followed by continuous stirring for 1 hr until homogeneous yellow viscous liquid was obtained. The molar ratio of bisphenol-A: formaldehyde: TETA was 1:4:1. The synthetic reaction is shown in Figure 4.1. After that the precursor was filled in a vial with seal and placed in an oven at 80°C for 72 hr into a close system yielding benzoxazine xerogel. The benzoxazine xerogel was then dried by ambient method and placed in an oven by using the fully curing step at 140, 160, 180 °C for 2 hr at each temperature and 200°C for 15 minutes in order to polymerize benzoxazine xerogel.

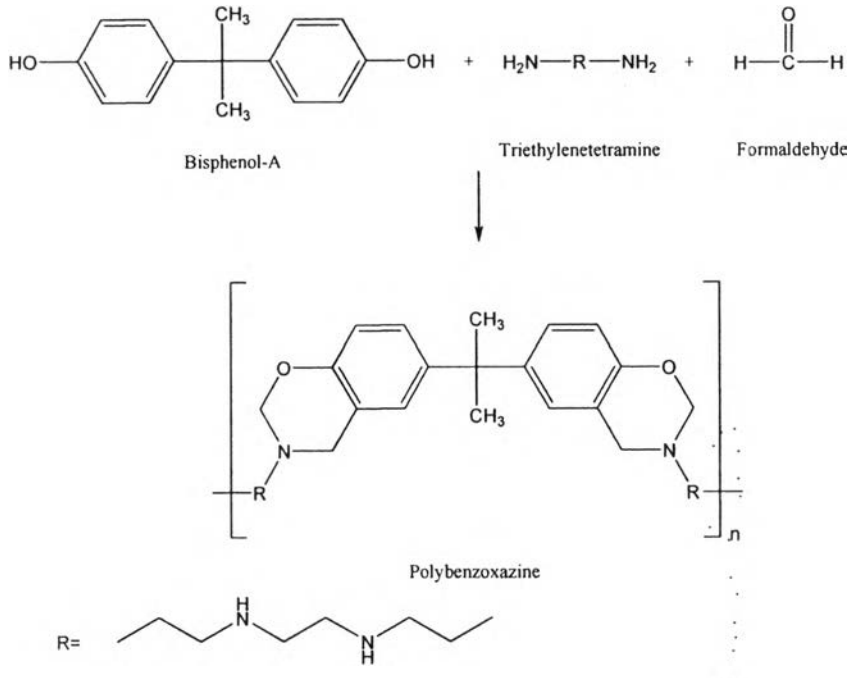

Figure 3.1 Preparation of polybenzoxazine precursor.

4.3.3.2 Preparation of Iron Oxide

The iron oxide (Fe_3O_4) was prepared by the following procedure: 4.80 g of $FeCl_3.6H_2O$ and 2.40 g of $FeCl_2.4H_2O$ were dissolved in 100 ml of deionized water under nitrogen gas. Next, 10 ml of NH_4OH (30%) was added at 80-90 °C and heated for 30 min. The black lump-like gel was separated by magnetic decantation and cooled to room temperature.

4.3.3.3 Preparation of Carbon Xerogel Electrodes

Benzoxazine xerogels were cut into the disc shape and pyrolyzed under a condition of nitrogen flow rate at 600 cm^3/min. The heating profile was used as follows: heating from room temperature to 250°C in 60 min, 250° to 600°C in 300 min, 600° to 800°C in 60 min and holding at 800°C for 120 min and finally cooling down to room temperature.

Heat–treated carbon xerogels (HCX) were prepared by using the heating profile at 300°C in air for 120 min to modify the electrode surface and to improve affinity with the electrolyte [7].

4.3.3.4 Preparation of Carbon Xerogel Composite Electrodes

The heat–treated carbon xerogel electrode discs with a thickness of 1 mm were impregnated in an iron oxide solution by varying the iron oxide content (1, 3, 5 %wt) and were then dried in a vacuum oven at 200 °C for 6 hr to remove solvent.

4.3.3.5 Characterization of Iron Oxide (magnetite) Polybenzoxazine Precursor and Carbon Xerogel Electrodes

X-ray diffraction (XRD) technique was used to characterize the crystallographic structure of iron oxide or magnetite (Fe_3O_4).

The chemical structure of benzoxazine precursor was characterized by Fourier Transform Infrared (FT-IR) spectroscopy. The thermal characteristics were measured using DSC and TG-DTA.

The surface area of carbon xerogels, heat–treated carbon xerogels were calculated from nitrogen adsorption isotherms at 77 K based on the Brunauer–Emmett–Teller (BET) method and the pore size distribution was calculated with the adsorption data based on the Barret-Joyner-Halenda method (BJH). The surface morphology, microstructure and EDX (energy dispersive X-ray) results were characterized using scanning electron microscope (SEM).

In case of electrochemical measurement, the galvanostatic charge/discharge, cyclic voltammetry (CV) and electrochemical impedance spectroscopy (EIS) were determined. All of the electrochemical measurements were performed at room temperature. The electrochemical test cell consisted of graphite sheets as current collectors, two carbon xerogels and/or carbon xerogel composite electrodes separated by microporous polyethylene membrane and 6M KOH solution. Moreover, in any measurement, the carbon xerogels and/or carbon xerogel composite electrodes were immersed in 6M KOH elecrolyte for 24 hr to ensure complete filling of the porous electrodes [2, 7].

4.4 Results and discussion

4.4.1 Thermal Characteristics of Polybenzoxazine Precursors

The curing behaviors of polybenzoxazine were examined by DSC. The DSC thermogram shows the broad exotherm at 238 °C as shown in Figure 4.1 due to the ring opening polymerization of cyclic benzoxazine precursor. After the precursor was fully polymerized, the exotherm completely disappeared indicating that the ring opening of oxazine ring was completed. This result was similar to that reported by Takeichi and coworker (2005).

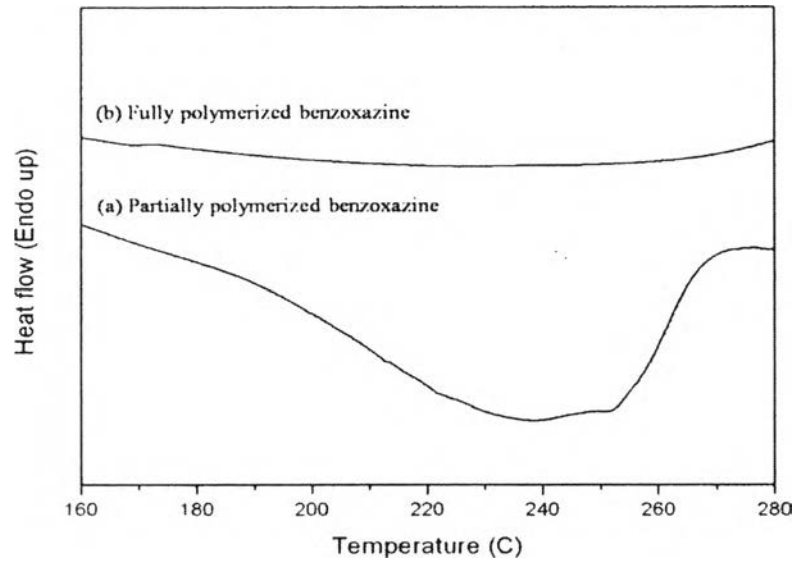

Figure 4.1 DSC thermograms of polybenzoxazine precursor.

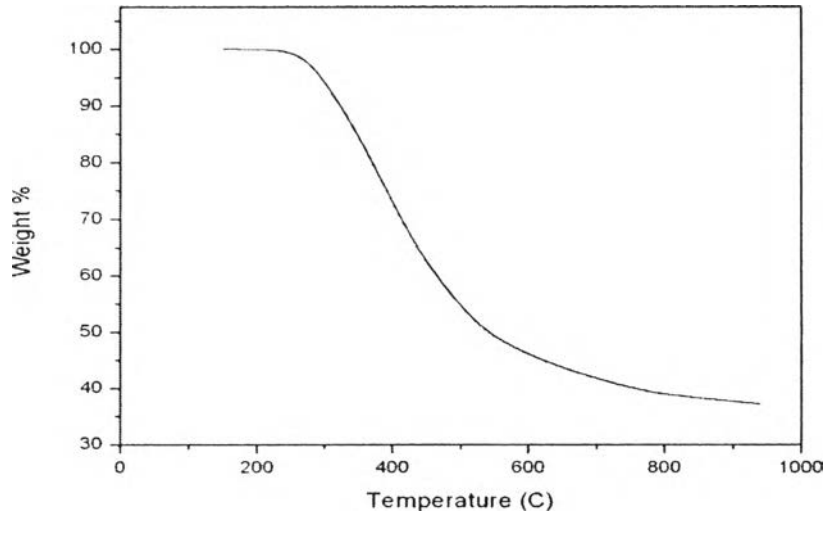

Figure 4.2 TGA thermogram of polybenzoxazine precursor.

Figure 4.2 shows the thermal stability of polybenzoxazine. The decomposition temperature began at 260 °C with the maximum mass loss rate in the temperature range of 260-600 °C. The result was in accordance with our previous study [1].

4.4.2 The Chemical Structure of Polybenzoxazine Precursors

The chemical structure of benzoxazine precursor was examined by FTIR spectra as shown in Figure 4.3. The characteristic absorption bands at 1234-1238 cm^{-1} (asymmetric stretching of C-O-C of oxazine), 1187 cm^{-1} (asymmetric stretch of C-N-C) and 1334-1340 cm^{-1} (CH_2 wagging) were observed (Figure 4.3(a)). Additionally, the characteristic absorption assigned to the stretching of trisubstituted benzene ring at 1511 cm^{-1} and the out-of-plane bending vibrations of C-H at 943-949 cm^{-1} were detected, indicating the presence of the cyclic benzoxazine structure in the backbone of the precursor [9]. After polymerization at 200 °C, the intensity of those characteristic absorption bands decreased due to the ring opening polymerization was completed as shown in Figure 4.3(b) [10].

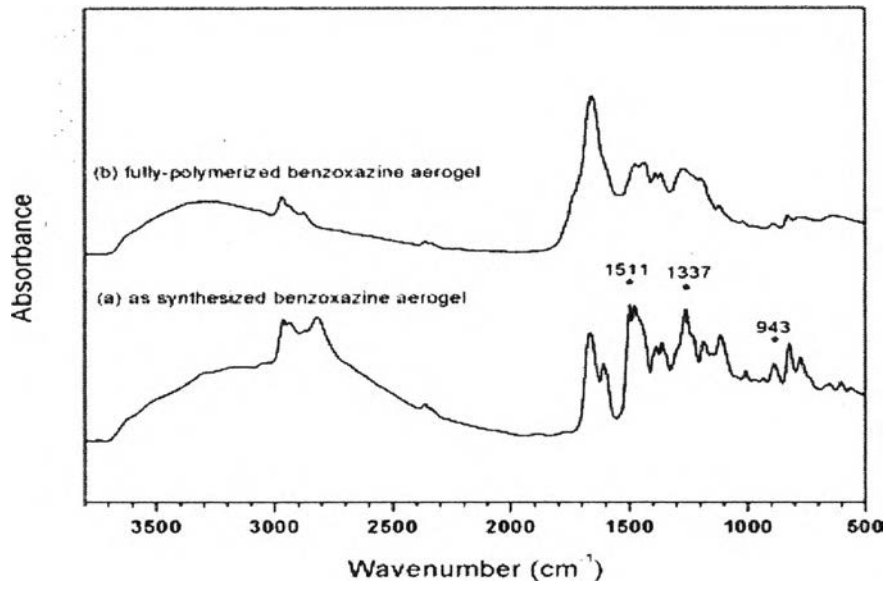

Figure 4.3 FTIR spectra of polybenzoxazine precursors.

4.4.3 Surface Characterization of Polybenzoxazine-Derived Carbon Xerogel

The surface area, pore volume and pore diameter of carbon xerogels are summarized in Table 4.1. It could be indicated that the surface area and porosity of the carbon xerogel with heat treatment in air at 300 °C were similar to the carbon

xerogel without heat treatment [7]. However, the heat–treated carbon xerogel had been presented the higher BET surface area than another that affected the specific capacitance of supercapacitor [11]. Apart from this, the pore diameter of all carbon xerogels prepared from polybenzoxazine precursor was in the range of 2-6 nm which was suitable for use as an electrode material in supercapacitors [7, 8].

Table 4.1 Surface area, pore volume and pore diameter of carbon xerogels prepared from benzoxazine precursor.

Parameter	CX	Heat–treated CX
BET surface area (m^2/g)	292	372
Total pore volume (cm^2/g)	0.27	0.29
Average pore size (nm)	3.67	3.08
Micropore volume (cm^3/g)	0.13	0.18
Mesopore volume (cm^3/g)	0.12	0.10
*Mesoporosity (%)	48.0	35.7
*Microporosity (%)	52.0	64.3

*Mesoporosity = (mesopore volume/total pore volume) × 100

*Microporosity = (micropore volume/total pore volume) × 100

4.4.4 Morphology of Carbon Xerogels, Heat–treated Carbon Xerogels, and Hybrid composites

The SEM micrographs in Figure 4.4 (a)-(d) show the porous structure of the carbon xerogels prepared from polybenzoxazine via ambient drying. The structure of the carbon xerogels without heat–treated at 300 °C in air composed of interconnected particles in three-dimension network containing continuous macropore, as shown in Figure 4.4(a) and (b), respectively. Figure 4.4 (c)-(d) reveal the heat–treated carbon xerogels prepared by heat treating the carbon xerogels in air at 300 °C for 2 hr. The micrograph also shows similar morphology compared with the carbon xerogels without heat treatment.

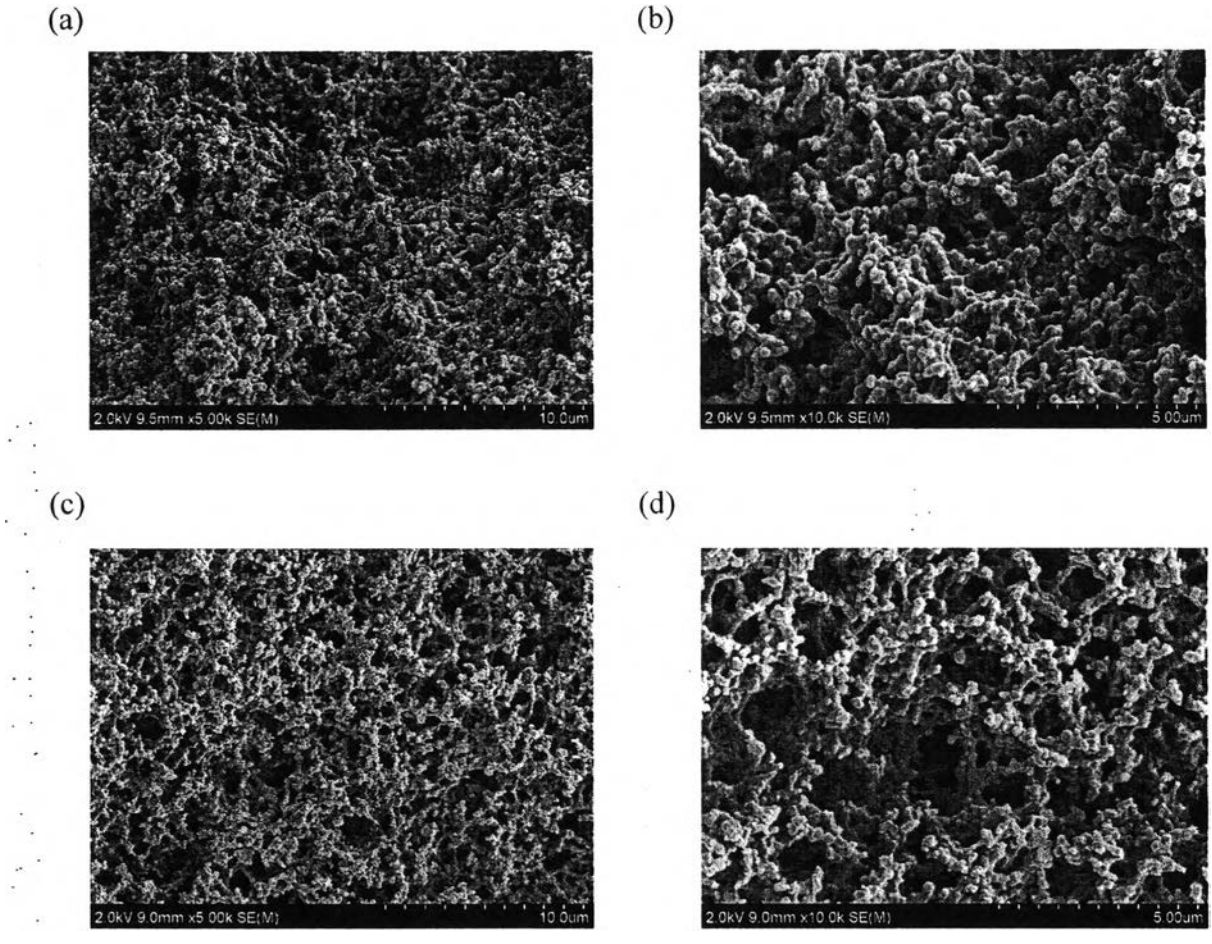

Figure 4.4 SEM micrographs of synthesized carbon xerogels: (a), (b) no heat treated, and (c), (d) heat treated at 300 °C in air.

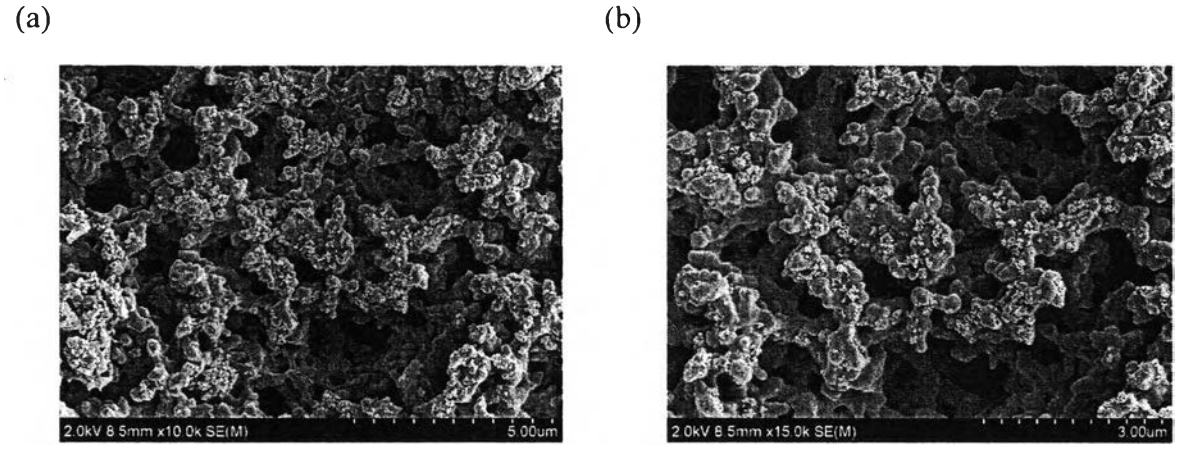

Figure 4.5 SEM micrographs of hybrid composite electrodes at different magnification: (a), (b) heat treated at 300 °C in air and impregnated with Fe_3O_4.

The heat–treated carbon xerogel electrode discs were impregnated in an iron oxide solution by varying the iron oxide content (1, 3, 5 %wt) and were then dried in a vacuum oven. Figure 4.5 (a)-(b) show the SEM images of the composite electrode, indicating that the Fe_3O_4-containing phase attached on the network structure of carbon particles.

4.4.5 Morphology and Characterization of Iron Oxide (Magnetite)

The prepared bare Fe_3O_4 nanopaticles (Figure 4.6) had the aggromerations due to the large free surface energy of each nanoparticle, which the aggregated particle consisting of average particle size of 6-17 nm. Figure 4.7 shows the X-ray diffraction (XRD) pattern of magnetite at (110), (220), (311), (400), (422), and (511), which are the characteristic peaks of the Fe_3O_4 crystal. The standard spectra for bulk magnetite are alike with the position and relative intensity of all diffraction peaks, except for broadening of the peaks. Fe_3O_4 can be oxidized to γ-Fe_2O_3 and can be additional changing into α-Fe_2O_3 at high temperature that the diffraction peaks at (113), (210), (213), and (210) are the characteristic peaks of γ-Fe_2O_3 and α-Fe_2O_3, respectively [12]. In this work, γ- Fe_2O_3 or α-Fe_2O_3, which could be assigned to impurities, were not detected. The particle size of the dried magnetite was characterized by the following XRD techniques. A Bruker D8 Advance X-ray diffractometer with Cu Kα radiation (λ = 0.154060 nm) in the 2θ interval of 10° to 80°, in steps of 0.02° operated at 40 kV and 30 mA was used in the XRD experiments. The average particle size of the samples was 14 nm, which was determined by using Scherrer's equation [13]:

$$D = \frac{0.9\ \lambda}{\beta \cos \theta} \qquad (1)$$

where D is the particle size (nm), λ is the wavelength of Cu Kα radiation (nm), and β is the broadening of the diffraction line measured at half the line maximum intensity (radian).

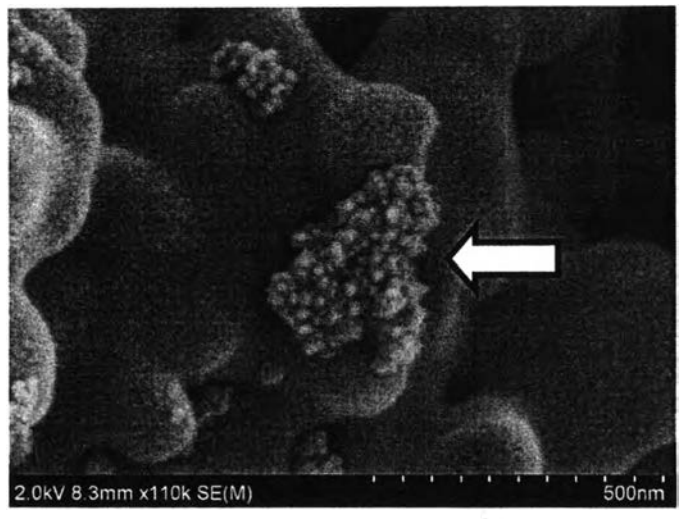

Figure 4.6 SEM micrograph of magnetite nanopaticles on the electrode surface (Fe_3O_4–impregnated on heat–treated carbon xerogels).

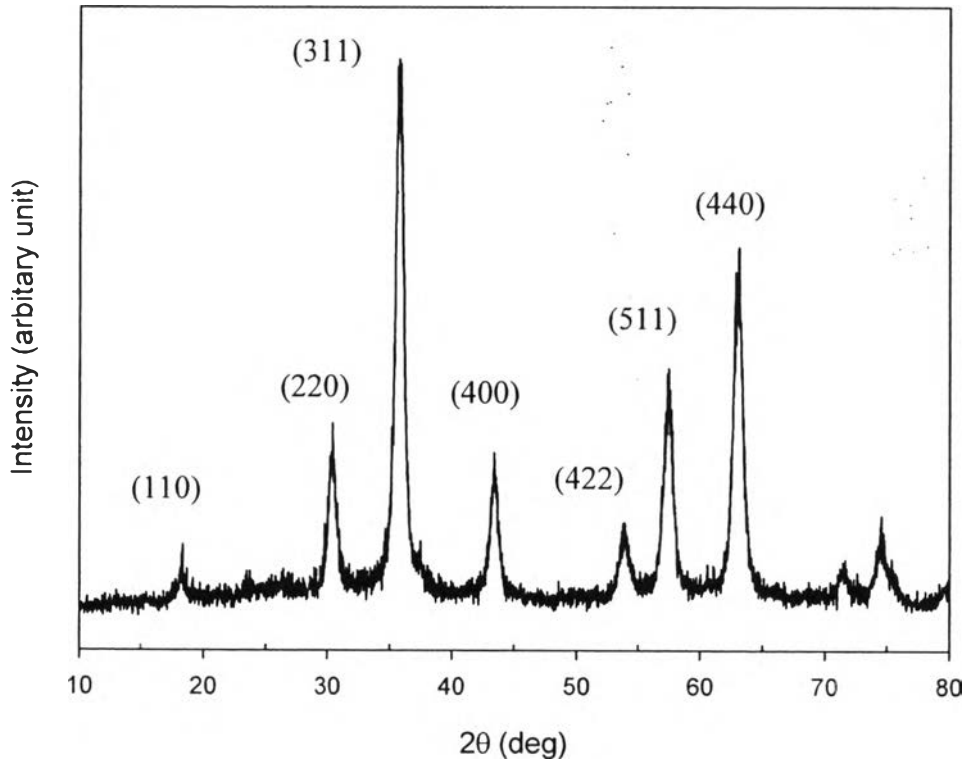

Figure 4.7 XRD patterns of the magnetite (Fe_3O_4) nanoparticles.

4.4.6 Electrochemical Characterizations

4.4.6.1 Cyclic Voltammetry Behaviors

The cyclic voltammograms of the carbon xerogel electrodes obtained at a scan rate of 1 and 5 mV/s in 6M KOH is shown in Figure 4.8. The figure indicated that the carbon xerogel electrodes with heat–treated at 300 °C in air exhibited excellent electrochemical performances confirmed by a rectangular-like shapes of cyclic voltammograms, as shown in Figure 4.8 (b), suggesting that ions occupied some pores within the electrode for the electrochemical double layer formation [14]. In addition, it also implies that the charge/discharge processes of the electric double layer are highly reversible [14, 15]. On the other hand, the cyclic voltammograms curves of non heat–treated carbon xerogels are smaller indicating that the charge/discharge processes of the electric double layer have low reversibility. As the scan rate increased (Figure 4.8 (a) and (b)), the rectangular shape became gradually depressed, because it was more difficult for the ions to transport into pores at a high scan rate [12, 16].

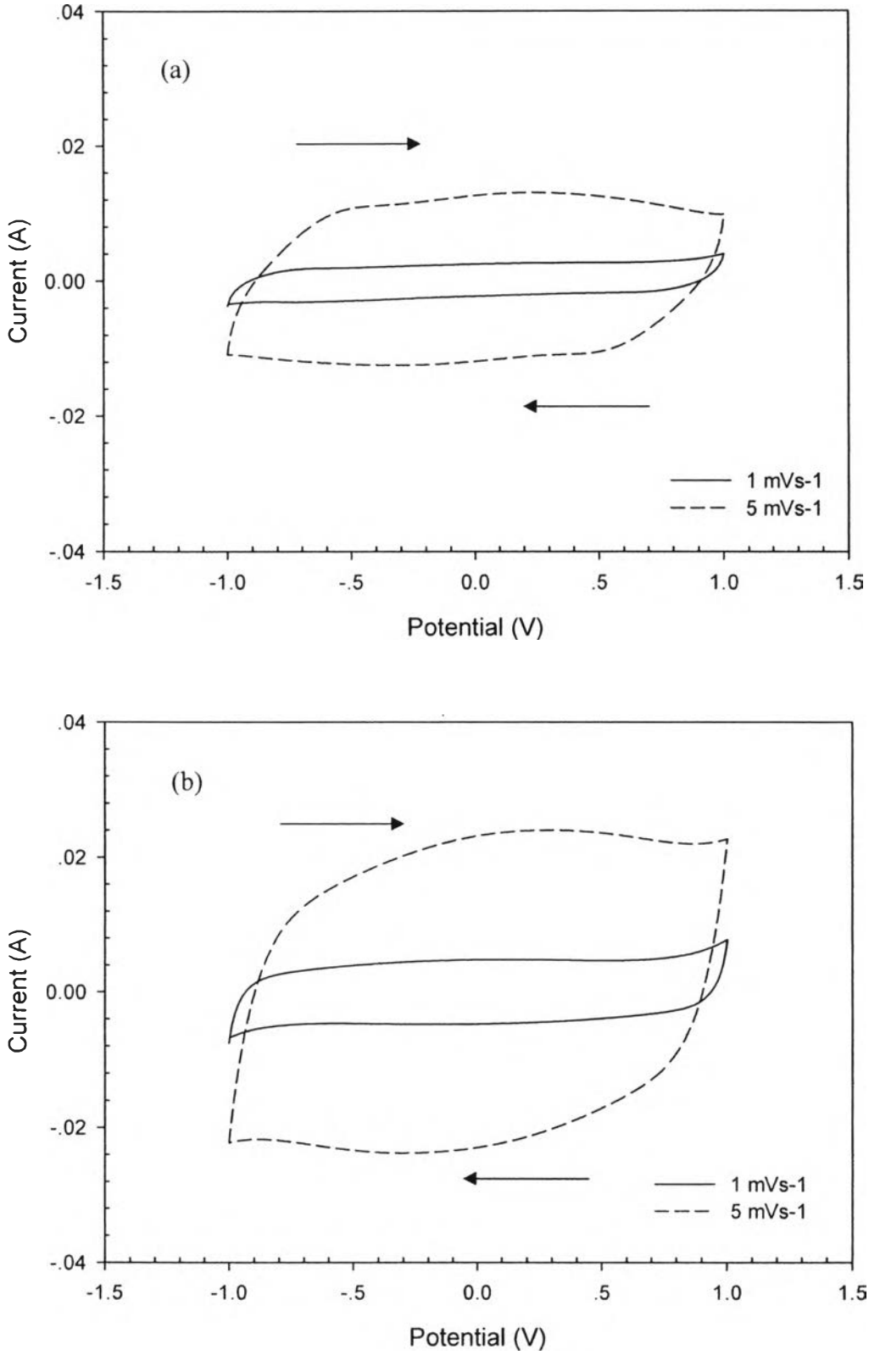

Figure 4.8 Cyclic voltammograms of carbon xerogel electrodes at a scan rate of 1 and 5 mV/s: (a) no heat treated and (b) heat treated at 300 °C in air.

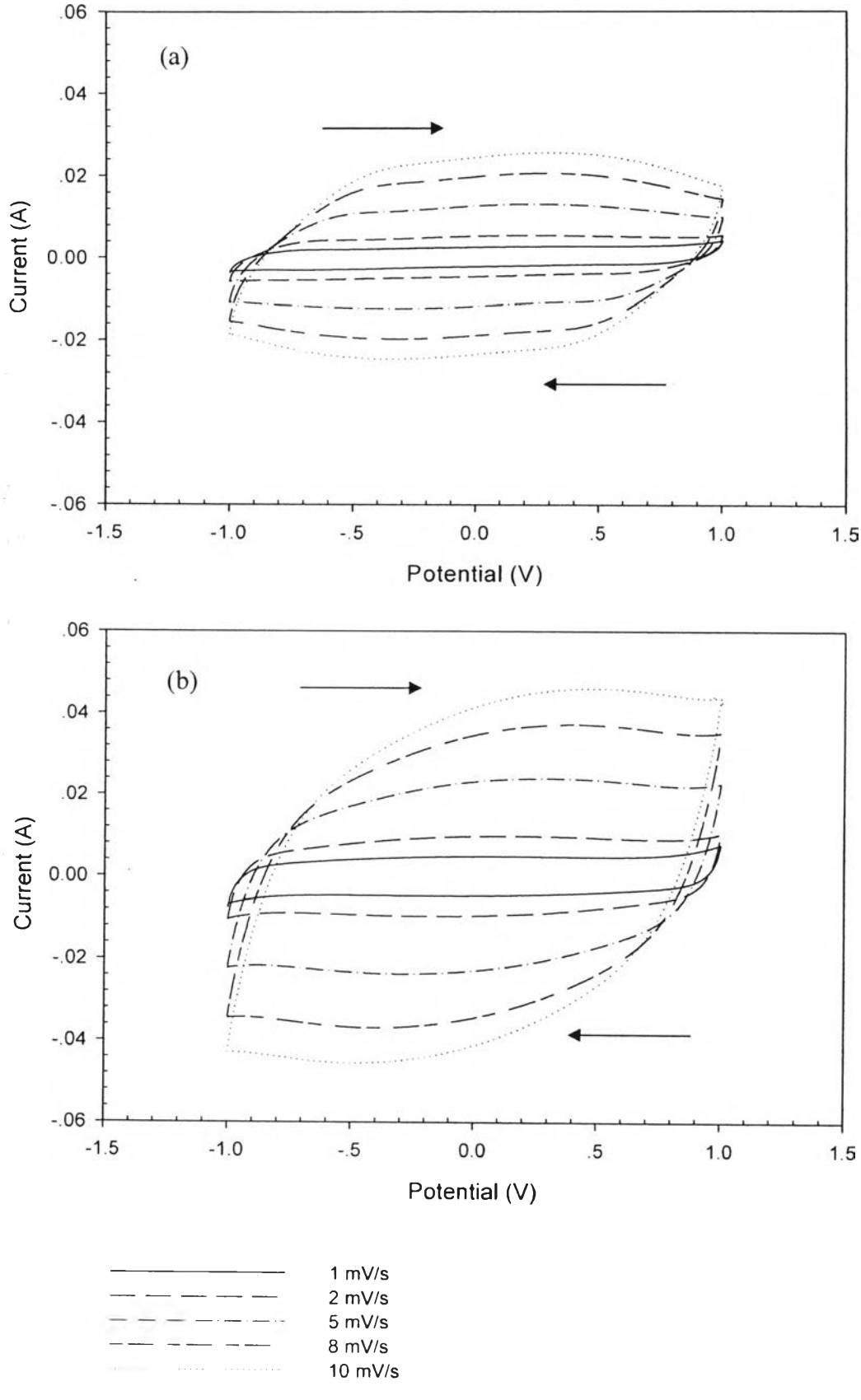

Figure 4.9 Cyclic voltammograms of carbon xerogel electrodes at a scan rate of 1, 2, 5, 8, and 10 mV/s: (a) no heat treated and (b) heat treated at 300 °C in air.

The difference of the non-Faradaic and Faradaic redox reactions can be considered by the cyclic voltammograms curves. Hybrid composite electrodes showed the pseudocapacitive behavior as seen in Figure 4.10 (the white arrow signs), indicating that the faradaic redox reactions occurred on the surface of impregnated iron oxide [5]. The cyclic voltammograms of Fe_3O_4–impregnated on heat–treated carbon xerogel electrodes with increasing iron oxide content (1, 3, and 5 wt.%) and different scan rates are presented in Figure 4.10 (a)-(c), which the symmetric peaks originating from the surface faradaic redox reactions were observed at scan rates of 1 to 10 mV/s. These peaks degraded gradually at high scan rates, similar to those observed in the case of pure carbon xerogel electrodes due to the difficulty of the ions transportation into pores [12, 16]. Although the hybrid composite electrodes showed the degradation of peaks, they exhibited quite stable cyclability, predicting long term electrochemical stability of iron oxide–impregnated on heat–treated carbon xerogels [5]. Moreover, the pseudocapacitive peaks were the most prominent at 3 wt.% Fe_3O_4–impregnated on electrodes as shown in Figure 4.10. These peaks ascended from faradaic-transfer reactions and electrostatic charging. The faradaic charge-discharge reaction in aqueous electrolyte is proposed in the equation below [2]:

$$FeO_x(OH)_y + \delta H^+ + \delta e^- \longleftrightarrow FeO_{x-\delta}(OH)_{y+\delta} \qquad (2)$$

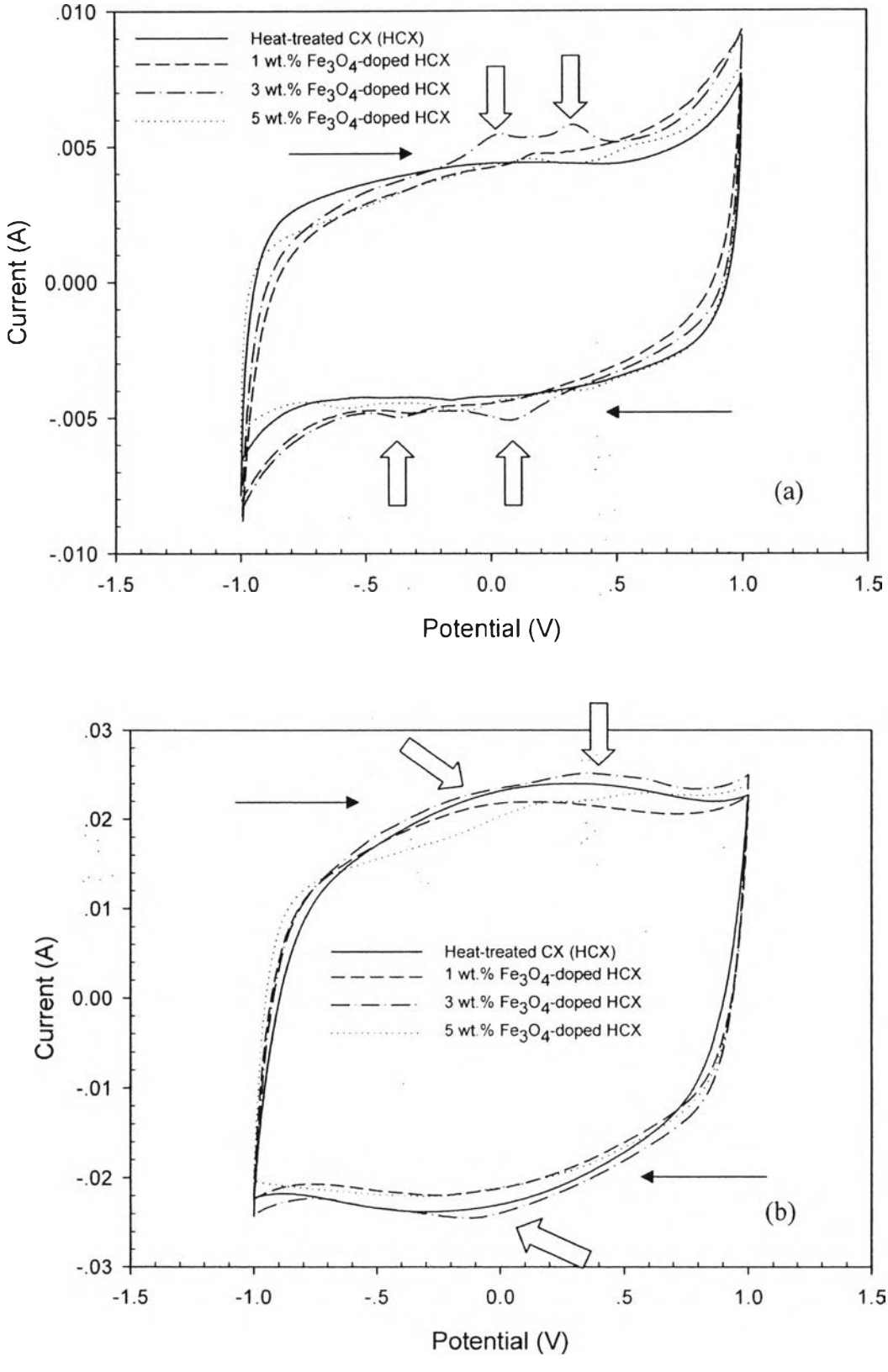

Figure 4.10 Cyclic voltammograms of 1, 3, and 5 wt.% Fe_3O_4–impregnated on heat–treated carbon xerogels at different scan rates: (a) scan rate = 1 mV/s, and (b) scan rate = 5 mV/s.

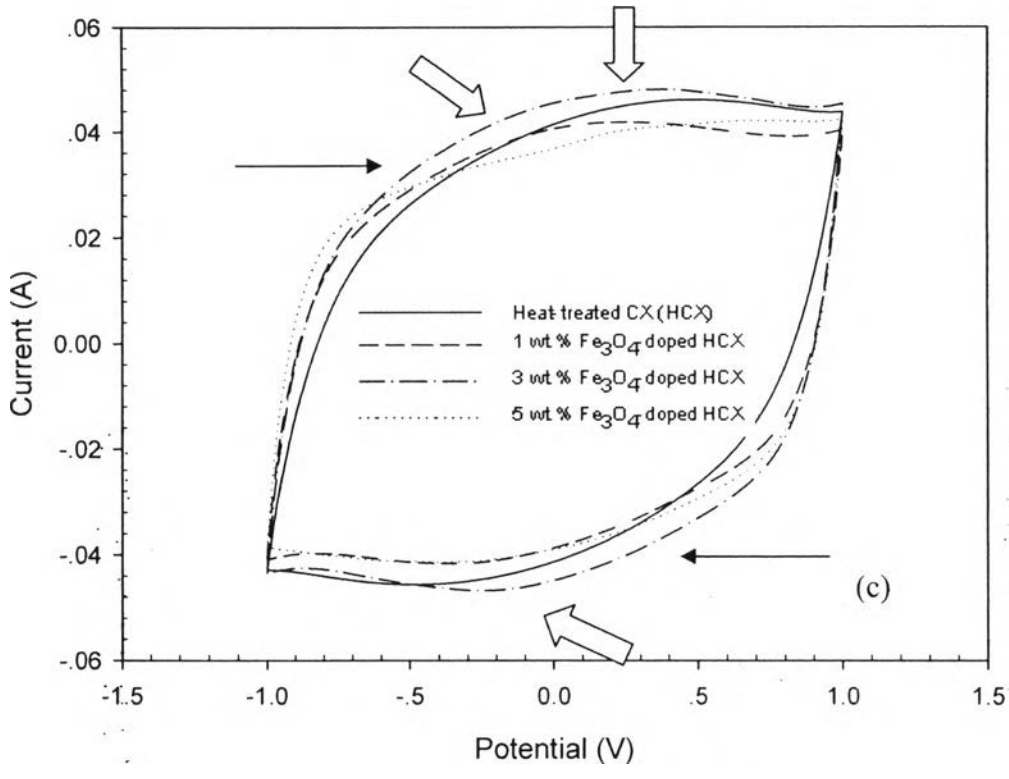

Figure 4.10 Cyclic voltammograms of 1, 3, and 5 wt.% Fe_3O_4–impregnated on heat–treated carbon xerogels at different scan rates: (c) scan rate = 10 mV/s.

4.4.6.2 Charge-Discharge Behaviors

The specific capacitance (C) of the carbon xerogel electrodes was calculated from the charge/discharge curve using the following equation [1, 7]:

$$C = \frac{i\Delta t}{m\Delta V} \qquad (3)$$

where C is the specific capacitance (F/g), I is the constant current (A), t is time period (s), ΔV is the potential difference (V) , and m is the mass of carbon xerogel electrode (g).

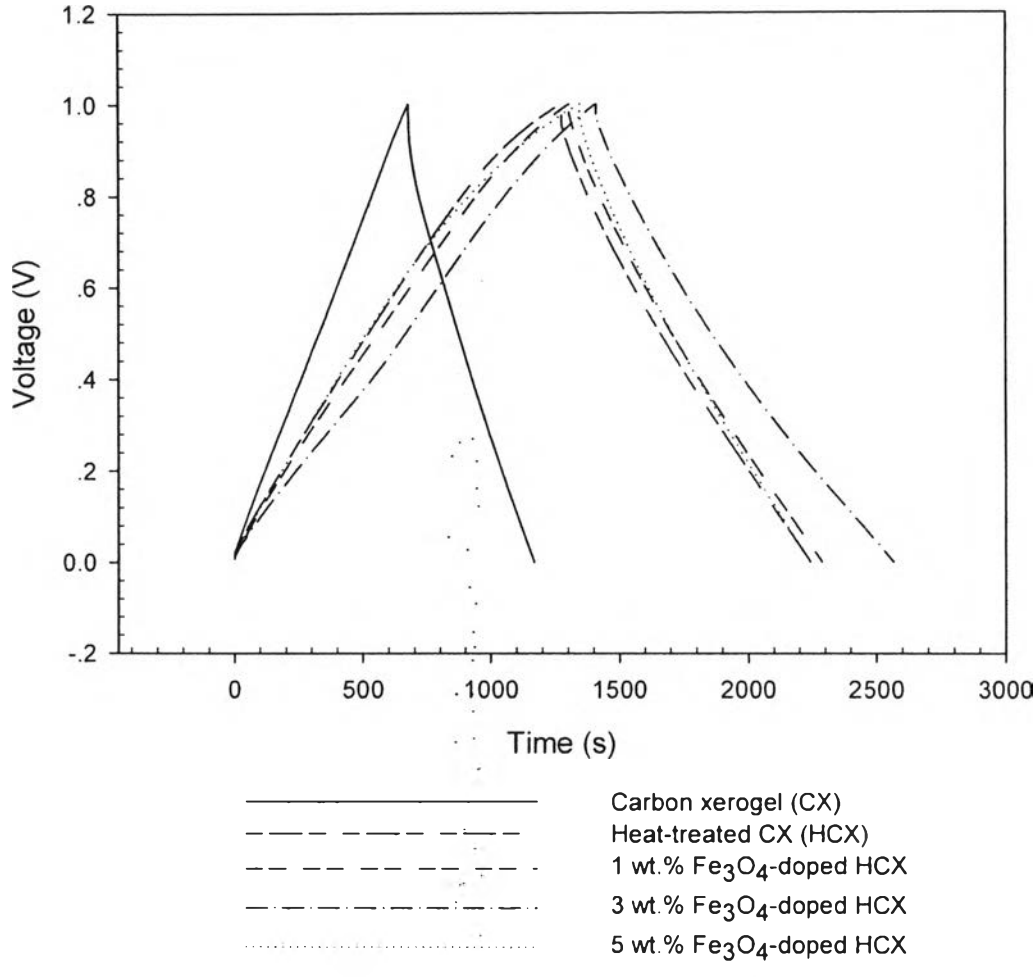

Figure 4.11 Charge/discharge curves of the carbon xerogel and hybrid composite electrodes measured at 5 mA/cm^2.

Table 4.2 The specific capacitance of carbon xerogel and hybrid composite electrodes calculated from discharge curves

Electrode	Specific capacitance (F/g)
Carbon xerogel	49.26
Heat–treated carbon xerogel (HCX)	108.25
1 wt.% Fe_3O_4–impregnated HCX	109.83
3 wt.% Fe_3O_4–impregnated HCX	120.27
5 wt.% Fe_3O_4–impregnated HCX	101.98

From Table 4.1, 4.2 and Figure 4.11, the heat–treated carbon xerogel at 300 °C in air had large amount of micropores along with high surface area; as a result, they showed higher specific capacitance than the one without heat treatment. Furthermore, the average pore diameter of the heat–treated carbon electrodes was approximately 3.08 nm, which was large enough and suitable for aqueous electrolyte to transport into pores to form the electrical double layer [8, 17, 18]. The higher surface area of the heat–treated carbon xreogels was generally a cause of the higher ability for charge accumulation; thereby, obtaining the higher specific capacitance of the carbon electrodes [19, 14]. However, it was rather difficult to make a conclusive summary on the parameters that affect the charge accumulation since the nature and the porosity of the precursor also play important roles [14, 20].

In case of hybrid composite electrodes, the highest specific capacitance was obtained from a sample of 3 wt.% Fe_3O_4–impregnated on heat–treated carbon xerogel due to its pseudocapacitive behavior from the surface faradaic redox reaction which was confirmed by the cyclic voltammograms curves. At 5 wt.% Fe_3O_4–impregnated on electrode surface, the specific capacitance was lower than the pure heat–treated carbon xerogel, implying that the partial mesoporous structure of carbon xerogel was blocked out from the exceeding particles of iron oxide. Therefore, it was more difficult for the electrolyte (6M KOH) ions to flow into the structure of mesopores. However, the presence of mesopores was necessary for the efficient charge propagation into the bulk of the electrode materials [21].

4.4.6.3 Electrochemical Impedance Characteristics

The frequency range of 10 kHz to 10 mHz was used to carry out the electrochemical impedance measurement and the potential difference of two electrodes was kept at 0 V during the measurement. The Nyquist plots for these electrodes are presented in Figure 4.9. At high frequency, the intercept of the semicircle on the left of the real axis (Z′) indicates the solution resistance, R_s, and the intercept on the right of the real axis indicates the sum of the polarization resistance or charge transfer resistance, R_{ct}, and the solution resistance, R_s. The diameter of the semicircle is equal to the charge transfer resistance, R_{ct},[22] which corresponds to

the charge transfer process, using redox couples in solution, at the electrode-electrolyte interface [23].

Figure 4.12 showed the solution resistance, R_s, of the electrochemical impedance spectrum which was similar in values, indicating that all carbon electrodes had similar solution resistance. However, the resistance did not play an essential role on the specific capacitance during the constant current charge-discharge cycling because the resistance has been excluded for the capacitance calculation [24]. Hsieh and Teng reported that the specific capacitance of carbon fabric increased significantly with the extent of oxidation, while the inner resistance (R_i), which means a small self-discharge of the electrode, also found to be increased with the extent of oxidation due to the local changes of charge density and the increase in redox activity [24].

At the high frequency of the plots in Figure 4.12, the semicircles can be easily detected representing the charge transfer resistance at the electrode/electrolyte interface. In addition, from the Nyquist plot, there was a similarity between the carbon xerogel electrodes with heat–treated and without heat–treated. This resemblance was the straight line inclined at an angle of around 90° to the real axis (Z′), which resulted from the diffusion of electrolyte ions within pores of the electrode [22, 25]. At low-frequency region, the imaginary part of the impedance for all carbon xerogel electrodes increased, showing the capacitive behavior of the supercapacitor [14, 20]. Moreover, these carbon xerogel electrodes exhibited a vertical line (90°) to the real axis, indicating an ideal capacitor behavior that has small diffusion resistance of electrolyte ions in the pore as a result of high specific capacitance [14, 22, 26]. The slope also related to dispersed resistance, R and capacitance, C, originated from various pore structures in carbon xerogels. This interpretation was called a "transmission line model" (Figure 4.13), reported by De Levie [27, 25, 28].

In case of the hybrid composite electrodes, the electrochemical impedance measurement is also shown in Figure 4.12 and Figure 4.14-4.16. The impregnation of iron oxide content with 1, 3 and 5 wt.% presented the internal resistance, R_i, about 1.5, 1.5 and 1.7 Ω, respectively. Apart from this, they had also smaller semicircles than the pure carbon xerogel electrodes in the

intermediate frequency regions. The charge transfer resistance, R_{ct}, of the electrode from the point of intercept with real axis in the high frequency range was estimated to be about 0.7, 1.2 and 0.5 Ω for 1, 3 and 5 wt.% Fe_3O_4–impregnated on heat–treated carbon xerogels, respectively. It could be deduced that Fe_3O_4 with the carbon powder enhanced the conductivity by reducing the internal resistance of electrodes [29] and the charge transfer resistance of the electrodes, while the charge transfer resistance of the pure carbon xerogel electrodes was about 2.7 Ω as shown in Figure 4.13. The redox reaction was a result of Fe_3O_4 that gives increase to pseudocapacitance and the double layer capacitance from the carbon matrix, including increasing the conductivity of the electrodes [29]. Furthermore, 3 wt.% Fe_3O_4–impregnated on heat–treated carbon xerogels had the largest semicircle than other hybrid composite electrodes, implying that a higher charge transfer resistance was the result of oxidation of magnetite surfaces under the highly alkaline condition to form an insulating Fe_2O_3 layer, which could be indicated by the irreversible oxidation process noticed during the oxidative scan near the high-potential end [30].

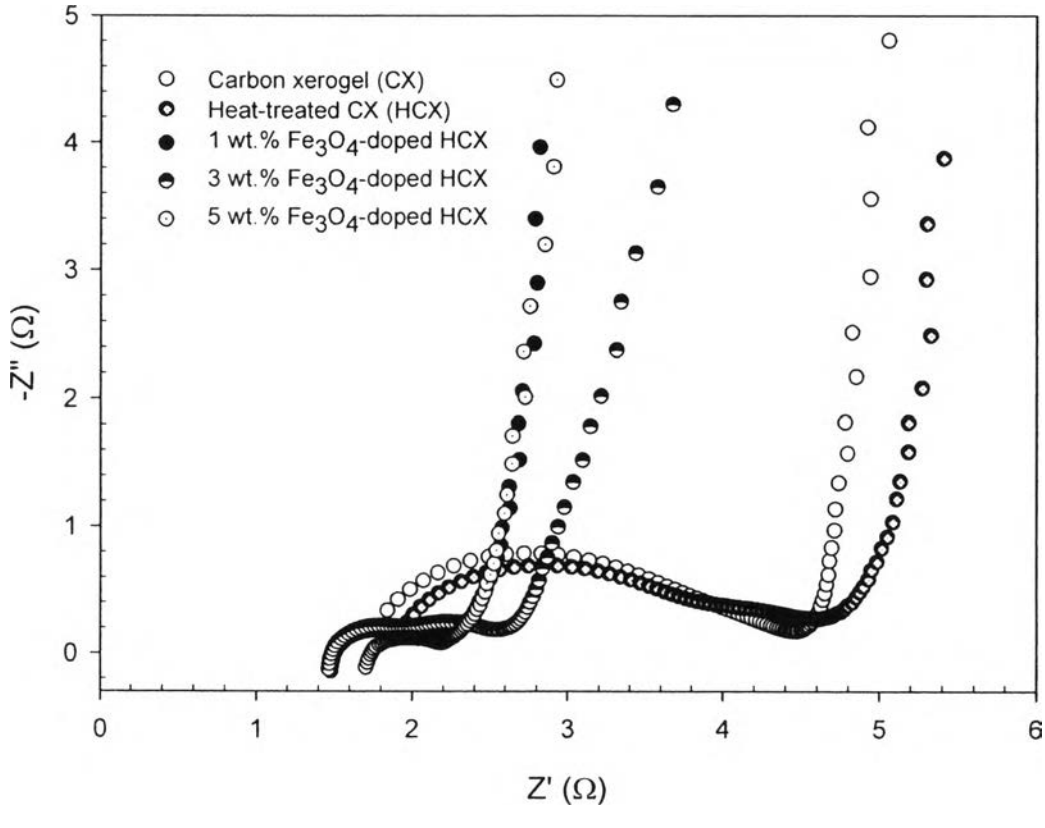

Figure 4.12 Nyquist plots for carbon xerogel and hybrid composite electrodes.

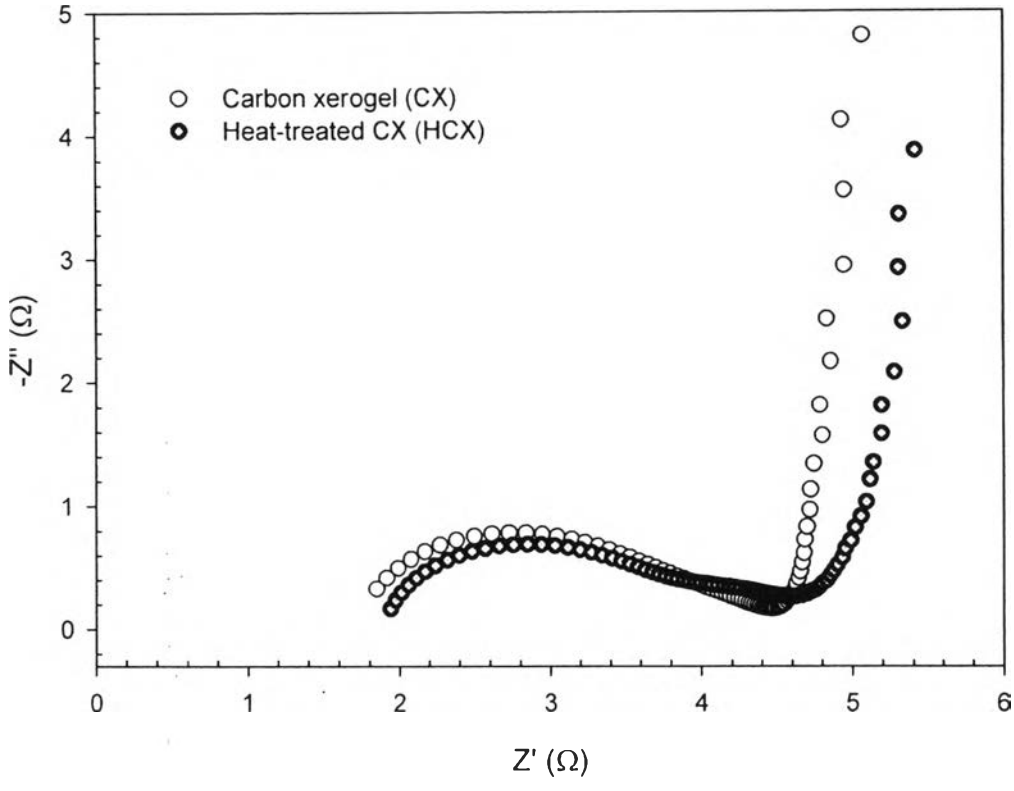

Figure 4.13 Nyquist plots for carbon xerogel and heat–terated carbon xerogel.

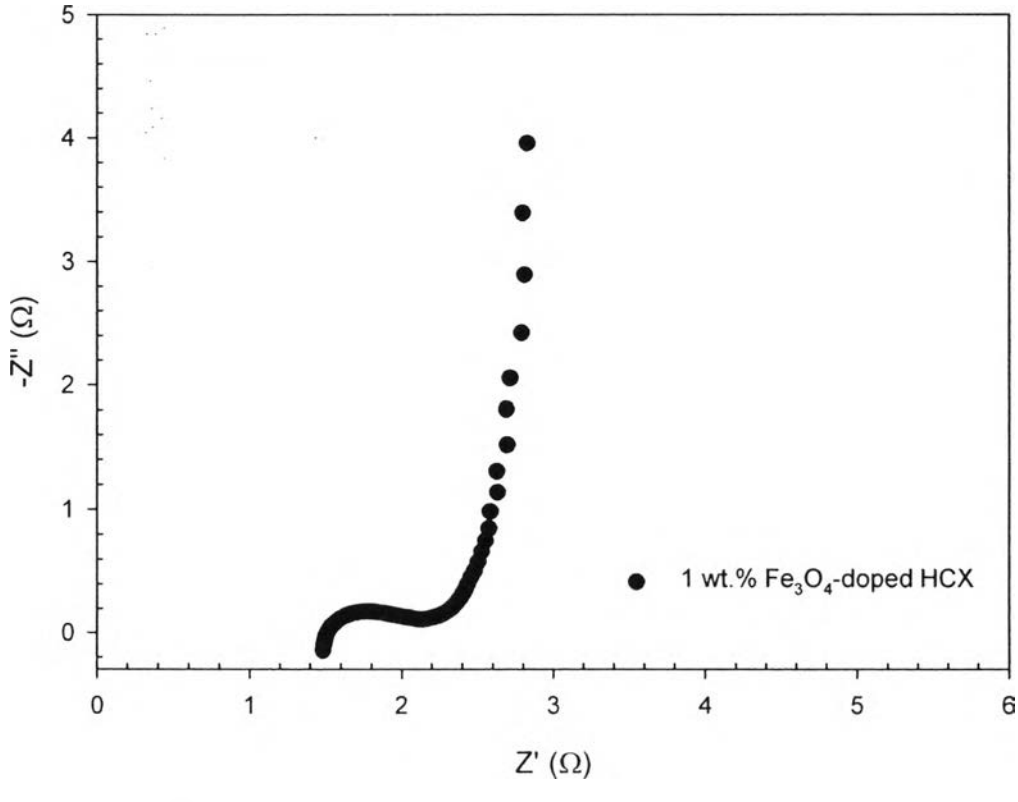

Figure 4.14 Nyquist plots of 1 wt% Fe_3O_4.–impregnated on heat–treated carbon xerogels.

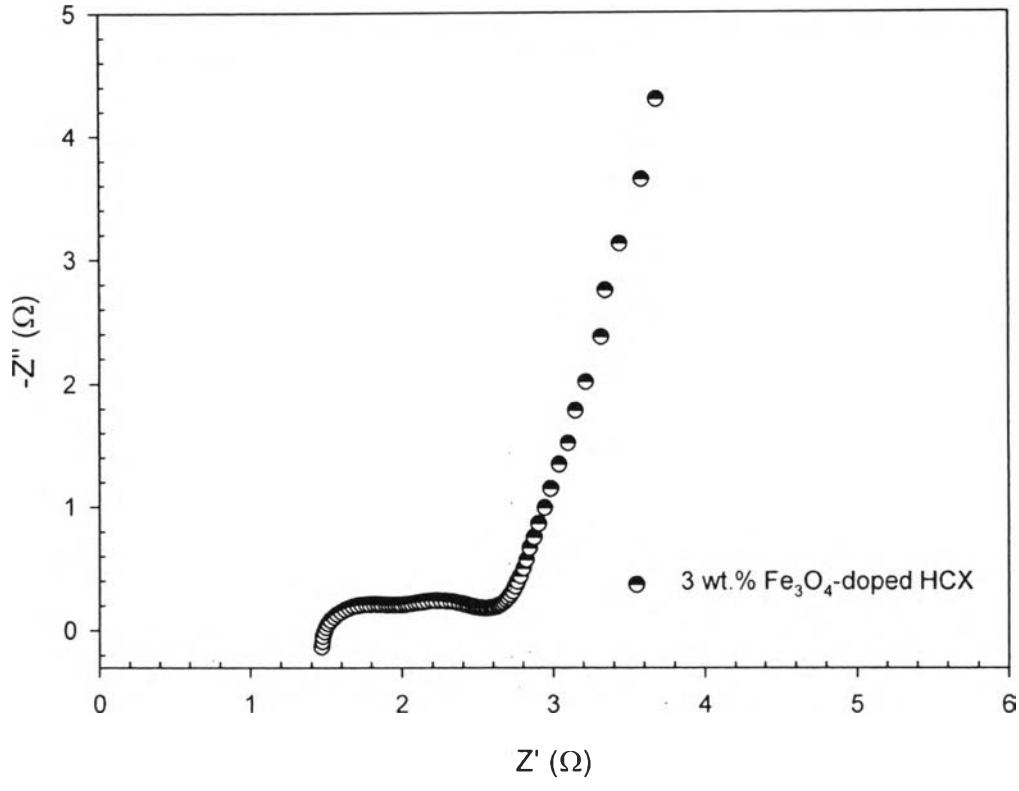

Figure 4.15 Nyquist plots of 3 wt% Fe_3O_4.–impregnated on heat–treated carbon xerogels.

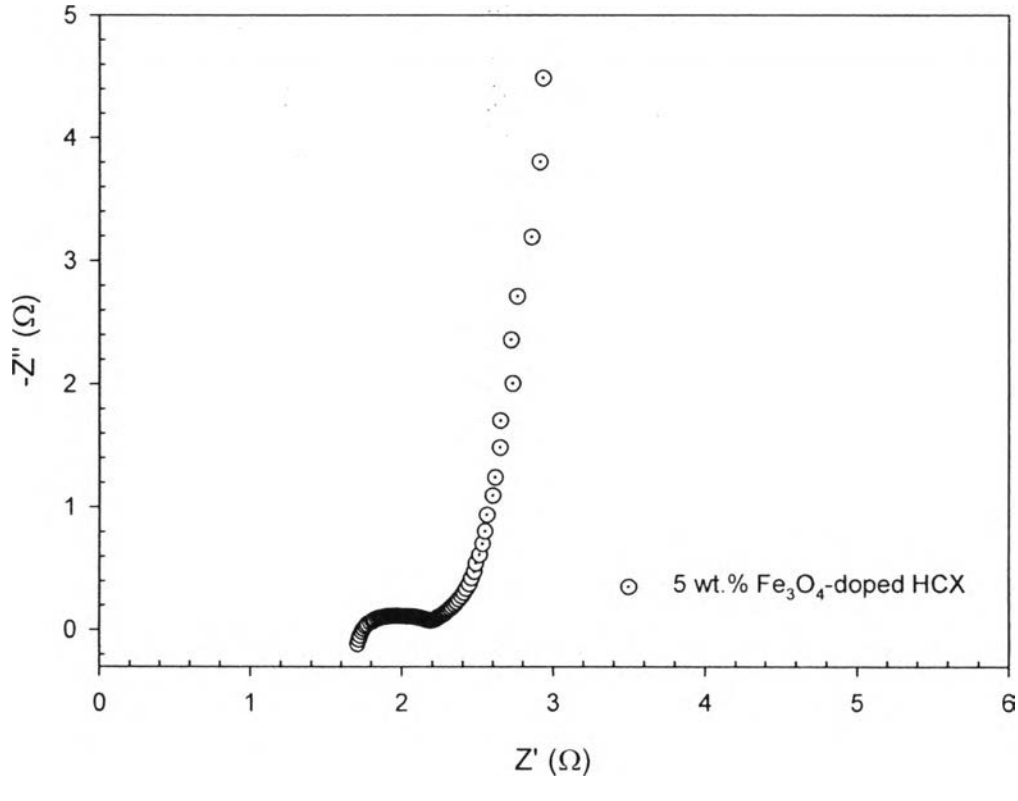

Figure 4.16 Nyquist plots of 5 wt% Fe_3O_4.–impregnated on heat–treated carbon xerogels.

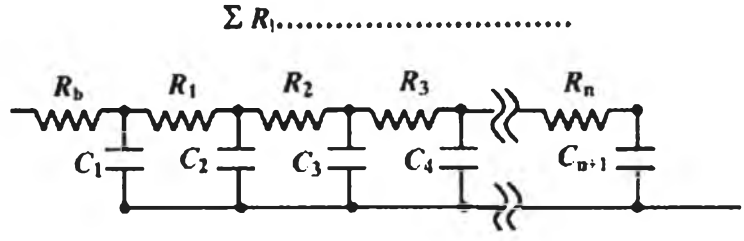

Figure 4.17 The equivalent circuit of carbon aerogel electrodes [28].

Conclusions

Electrodes of supercapacitor have been prepared using carbon xreogel, which were synthesized via ambient drying by using polybenzoxazine as a precursor. Carbon xerogel electrodes showed good electrochemical performances and the heat–treated carbon xerogel electrodes has higher capacitance than the electrodes without heat treatment due to its high useable surface area for electrical double layer formation.

Iron oxide/Carbon xerogel nanocomposites were successfully obtained by the impregnation method with a variation of iron oxide (Fe_3O_4) content and the supercapacitor performances were evaluated. The impregnation of iron oxide onto carbon xerogels has significantly improved the energy storage capability of these high surface area materials. The specific capacitance of hybrid composite electrodes was measured according to the galvanostatic charge/didcharge method. The electrode prepared by loading 3 wt% of Fe_3O_4 on heat–treated caebon xerogels exhibited the highest capacitance and quite stable cyclability. This high specific capacitance was attributed to the pseudocapacitance effect from the surface faradaic redox reaction. However, the energy storage process of these new materials was limited by mass transport of electrolyte ions in the pores of the carbon xerogel if the content of Fe_3O_4 was further increased.

Acknowledgements

This thesis work is funded by the Petroleum and Petrochemical College, and the National Center of Excellence for Petroleum, Petrochemicals, and Advanced Materials, Thailand. We would like to thank Associate Professor Suwabun Chirachanchai for the electrochemical measurements.

References

[1] Katanyoota, P., Chaisuwan, T., Wongchaisuwat, A., and Wongkasemjit, S. (2010). Novel polybenzoxazine-based carbon aerogel electrode for supercapacitors. Journal of Materials Science and Engineering B, 167, 36-42.

[2] Hwang, S.W., and Hyun, S.H. (2007). Synthesis and characterization of tin oxide/carbon aerogel composite electrodes for electrochemical supercapacitors. Journal of Power Sources, 172, 451-459.

[3] Pekala, R.W., Alviso, C.T., Kong, F.M., and Hulsey, S.S. (1992). Aerogels derived from multifunctional organic monomers. Journal of Non-crystalline Solids, 145, 90-98.

[4] Wei, Y.-Z., Frang, B., Iwasa, S., and Kumagai, M. (2005) A novel electrode material for electric double-layer capacitors. Journal of Power Sources, 141, 386-391.

[5] Lee, Y.L., Jung, J.C., Park, S., Seo, J.G., Baeck, SH.,Yoon, J.R., Yi., J., and Song, I.K. (2010). Preparation and characterization of metal-doped carbon aerogel for supercapacitor. Journal of Current Applied Physics, 10, 947-951.

[6] Ghosh, N.N., Kiskan, B., and Yagci Y. (2007). Polybenzoxazines — New high performance thermosetting resins: Synthesis and properties. Progress in Polymer Science, 32, 1344-1391.

[7] Kim, S.J., Hwang S.W., and Hyun S.H. (2005) Preparation of carbon aerogel electrodes for supercapacitor and their electrochemical characteristics. Journal of Material Science, 40, 725-731.

[8] Hwang, S.W. and Hyun, S.H. (2004) Capacitance control of carbon aerogel electrode. Journal of Non-Crystalline Solids, 347, 238-245.

[9] Dunkers, J. and Ishida, H. (1995) Vibrational assignments of N,N-bis(3,5-dimethyl-2-hydroxybenzyl)methylamine in the fingerprint region. Spectro-chimica Acta Part A: Molecular and Biomolecular Spectroscopy, 51, 1061-1074.

[10] Takeichi, T., Kano, T., and Agag, T. (2005). Synthesis and thermal cure of high molecular weight polybenzoxazine precursors and the properties of the thermosets. Polymer, 46, 12172–12180.

[11] Wang, J., Zhang, S.Q., Guo, Y.Z., Shen, J., Attia, S.M., Zhou, B., Zheng, G.Z., and Gui, Y.S. (2001). Morphological effects on the electrical and

electrochemical properties of carbon aerogels. Journal of the Electrochemical Society, 148, D75-D77.

[12] Liu, X., Kaminski, M.D., Guan, Y., Chen, H., Liu, H., and Rosengart, A.J. (2006). Preparation and characterization of hydrophobic superparamagnetic magnetite gel. Journal of Magnetism and magnetic materials, 306, 248-253.

[13] Yazdania, F., and Edrissi M. (2010). Effect of pressure on the size of magnetite nanoparticles in the coprecipitation synthesis. Materials Science and Engineering B, 171, 86–89.

[14] Li, J., Wang, X., Wang, Y., Huang, Q., Dai, D., Gamboa, S., and Sebastian, P.J. (2008). Structure and electrochemical properties of carbon aerogels synthesized at ambient temperatures as supercapacitors. Journal of Non Crystalline Solids, 354, 19-24.

[15] Prabaharan, S.R.S., Vimala, R., and Zainal, Z. (2006) Nanostructured meso-porous carbon as electrodes for supercapacitors. Journal of Power Sources, 161, 730-736.

[16] Xia, K., Gao, Q., Jiang, J., and Hu, J. (2008) Hierarchical porous carbons with controlled micropores and mesopores for supercapacitor electrode materials. Carbon, 46, 1718-1726.

[17] Frackowiak, E., and Béguin, F. (2001). Review Carbon materials for the electrochemical storage of energy in capacitors. Carbon, 39, 937-950.

[18] Wang, J., Yang, X., Wu, D., Fu, R., Dresselhaus M.S., and Dreaaelhaus G. (2008). The porous structures of activated carbon aerogels and their effects on electrochemical performance. Journal of Power Sources, 185, 589-594.

[19] Li, W., Pröbstle, H., and Fricke, J. (2003). Electrochemical behavior of mixed CmRF based carbon aerogels as electrode materials for supercapacitors. Journal of Non-Crystalline Solids, 325, 1-5.

[20] Gamby, J., Taberna, P.L., Simon, P., Fauvarque, J.F., and Chesneau, M. (2001) Studies and characteristics of various activated carbons used for carbon/carbon supercapacitors. Journal of Power Sources, 101, 109-116.

[21] Meng, Q.H., Liu, L., Song, H.H., Zhang, R., and Ling, L.C. (2004). Electrochemical properties of carbon aerogels electrode for super-capacitor. Journal of Inorganic Materials, 19(3), 593-598.

[22] Liu, X., Zhang, R., Zhan, L., Long, D., Qiao, W., Yang, J., and Ling, L. (2007) Impedance of carbon aerogel/activated carbon composites as electrodes of electrochemical capacitors in aprotic electrolyte. New Carbon Materrials, 22, 153-158.

[23] Dandekar, M.S., Arabale, G., and Vijayamohanan, K. (2005) Preparation and characterization of composite electrodes of coconut-shell-based activated carbon and hydrous ruthenium oxide for supercacitors. Journal of Power Sources, 141, 198-203.

[24] Hsieh, C. and Teng, H. (2002) Influence of oxygen treatment on elecric double-layer capacitance of activated carbon fabrics. Carbon, 40, 667-674.

[25] Honda, Y., Haramoto, T., Takeshige, M., Chiozaki, H., Kitamura, T., and Ishikawa, M. (2007) Aligned MWCNT sheet electrodes prepared by transfer methodology providing high-power capacitor performance. Electrochemical and Solid State Letters, 10, A106-A110.

[26] He, X., Lei, J., Geng, Y., Zhang, X., Wu, M., and Zheng, M. (2009). Preparation of microporous activated carbon and its electrochemical performance for electric double layer capacitor. Journal of Physics and Chemistry of Solids, 70, 738-744.

[27] Fang, B. and Binder, L. (2006). A modified activated carbon aerogel for high-energy storage in electrical double layer capacitors. Journal of Power Sources, 163, 616-622.

[28] R. de Levie. (1963) On Porous Electrodes in Electrolyte Solutions. Electrochemica Acta, 8, 751-780.

[29] Kalpana, D., Omkuma, K.S., Suresh Kumar, S., and Renganathan, N.G. (2006). A novel high power symmetric ZnO/carbon aerogel composite electrode for electrochemical supercapacitor. Electrochemica Acta, 52, 1309-1315.

[30] Du, X., Wang, C., Chen, M., Jiao, Y., and Wang, J. (2009). Electrochemical performances of nanoparticle Fe3O4/activated carbon supercapacitor using KOH electrolyte solution. Journal of Pysical Chemistry Part C, 113, 2643-2646.